Heliyon 11 (2025) e41696

Contents lists available at ScienceDirect

Heliyon

journal homepage: www.cell.com/heliyon

Research article

Maximizing zearalenone removal: Unveiling the superior efficiency of pre-treated carbon in adsorption and photocatalysis

J.C. Gómez-Vilchis [a], G. García-Rosales [a,*], L.C. Longoria-Gándara [b], E.O. Pérez-Gómez [a], D. Tenorio-Castilleros [c]

[a] National Technological Institute of Mexico, Toluca Technological Institute, Postgraduate Department in Environmental, Nanotechnology Laboratory, Technological Avenue 100 s/n, Colonia Agrícola, Bellavista, La Virgen, 52149, Metepec, Mexico
[b] Division for Latin America, Department of Technical Cooperation International Atomic Energy Agency, Wagramer Strasse 5, P.O. Box 100, A-1400, Vienna, Austria
[c] National Institute of Nuclear Research, Chemistry Department, Chemistry Laboratory, Technological Avenue 100 s/n. Colonia Agrícola, Bellavista, La Virgen, 52149, Metepec, Mexico

ARTICLE INFO

Keywords:
Adsorption
Photocatalysis
Zearalenone
Mycotoxins
Carbon

ABSTRACT

Zearalenone (ZEN) is a mycotoxin produced by *Fusarium* species, commonly found in food, feed, and water bodies. Due to its classification as a carcinogen, ZEN is a hazardous contaminant that requires removal from aqueous and food-related effluents. To prevent its release into aquatic systems, effective tertiary treatment methods are essential. This study investigates the removal of ZEN using two advanced water treatment technologies: adsorption and photocatalysis. Two carbonaceous materials derived from avocado seed residues (BC and BCA) were synthesized and characterized using SEM, BET, and XPS techniques. The adsorption capacity of BC was determined to be 60.23 μg g^{-1}, while BCA exhibited a capacity of 64.96 μg g^{-1}, as modeled by the Freundlich isotherm. Both materials achieved ZEN removal efficiencies of 65 ± 5 % for BC and 70 ± 5 % for BCA, influenced by pH, temperature, and initial concentration. Photodegradation results showed removal efficiencies of 95 ± 0.68 % for BC and 98 ± 0.36 % for BCA, highlighting the critical role of light intensity in ZEN degradation. This study underscores the potential of BC and BCA for ZEN removal through advanced water treatment technologies, representing a significant step towards sustainable and environmentally friendly remediation. Furthermore, the adsorption process demonstrated reusability over 17 cycles, while the photocatalytic process showed promise for long-term and sustainable use, with up to 20 reuse cycles.

1. Introduction

Emerging contaminants such as pharmaceuticals [1–4], organic compounds [5–8], mycotoxins, and other substances pose a growing challenge to water quality and public health due to their persistence and toxic effects on ecosystems. Consequently, the removal of these contaminants from water bodies has gained significant attention in recent years due to their adverse environmental and health impacts. One promising strategy for water purification involves advanced adsorbents [3,9,10], including metal-organic frameworks (MOFs) [10,11], hybrid materials [12], and biochars [13]. Mycotoxins are low-molecular-weight secondary

* Corresponding author.
E-mail address: gegaromx@yahoo.com.mx (G. García-Rosales).

https://doi.org/10.1016/j.heliyon.2025.e41696
Received 28 August 2024; Received in revised form 16 December 2024; Accepted 3 January 2025
Available online 9 January 2025

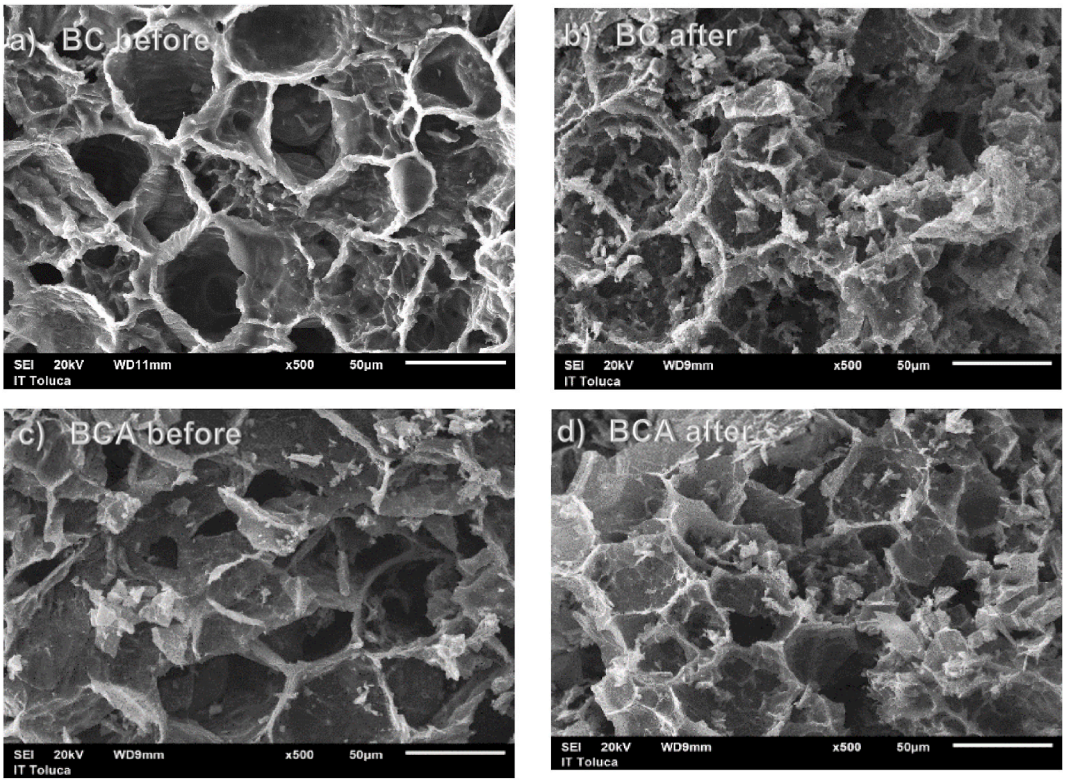

Fig. 1. Microscopic images depicting: (a) BC, (b) BC following ZEN adsorption, (c) BCA, and (d) BCA following ZEN adsorption.

metabolites produced by fungi such as *Aspergillus*, *Penicillium*, *Alternaria*, *Claviceps*, and *Fusarium* [14]. Among these, *Fusarium* species are notable for producing zearalenone (ZEN), a mycotoxin classified as a Group III carcinogen by the International Agency for Research on Cancer (IARC) [15]. ZEN presents serious risks due to its estrogenic, genotoxic, immunotoxic, and hepatotoxic properties [16], with its metabolites, α- and β-zearalenol (ZEL), exacerbating these effects α-ZEL being the most active. Despite ZEN's low solubility, its presence in surface and wastewater is concerning as it impacts aquatic ecosystems and groundwater quality, affecting the development of species such as fish and birds [16–19]. This highlights the urgent need to implement advanced treatment methods to effectively remove ZEN and other emerging contaminants that challenge conventional purification systems. Although various methods such as adsorption, photocatalysis, and biological treatments have been explored [20], this study presents an innovative approach by synergistically integrating adsorption and photocatalysis. Adsorption is valued for its simplicity and efficiency, while photocatalysis is renowned for its oxidative potential and rapid reaction capacity [21,22]. Together, these methods provide a promising alternative for the comprehensive and efficient removal of contaminants like ZEN.

The innovation of this research lies in the development of multifunctional carbonaceous materials derived from Hass avocado seeds, a waste product of the avocado industry. Unlike previous studies that employed higher doses of adsorbent materials or focused on single remediation techniques, this study investigates biochar (BC) and chemically activated biochar (BCA) produced from avocado seeds to achieve high ZEN removal efficiency using significantly lower doses. This approach not only enhances the practical application and sustainability of the materials but also offers an environmentally friendly solution by utilizing an underutilized biomass resource.

Mexico, one of the leading producers of Hass avocados, generates large quantities of seeds comprising 16 % of the fruit's weight that are typically discarded [23,24]. Transforming these seeds into high-value carbon materials provides dual environmental and economic benefits. Furthermore, this study pioneers the integration of chemical pretreatment to enhance biochar performance, optimizing surface properties for improved adsorption and photocatalytic activity. By investigating key operational factors such as contact time, initial pH, ZEN concentration, temperature, and the influence of ultraviolet light wavelength, this research provides a comprehensive assessment of the adsorption and photocatalytic degradation mechanisms of ZEN.

2. Methodology

2.1. Synthesis of carbonaceous materials (BC and BCA)

Hass avocado (*Persea americana*) seeds were collected, thoroughly washed, and dried in an oven at 45 °C for three days. The outer seed coat was removed, and the seeds were ground to achieve a particle size of 0.83 mm. The ground material was washed with

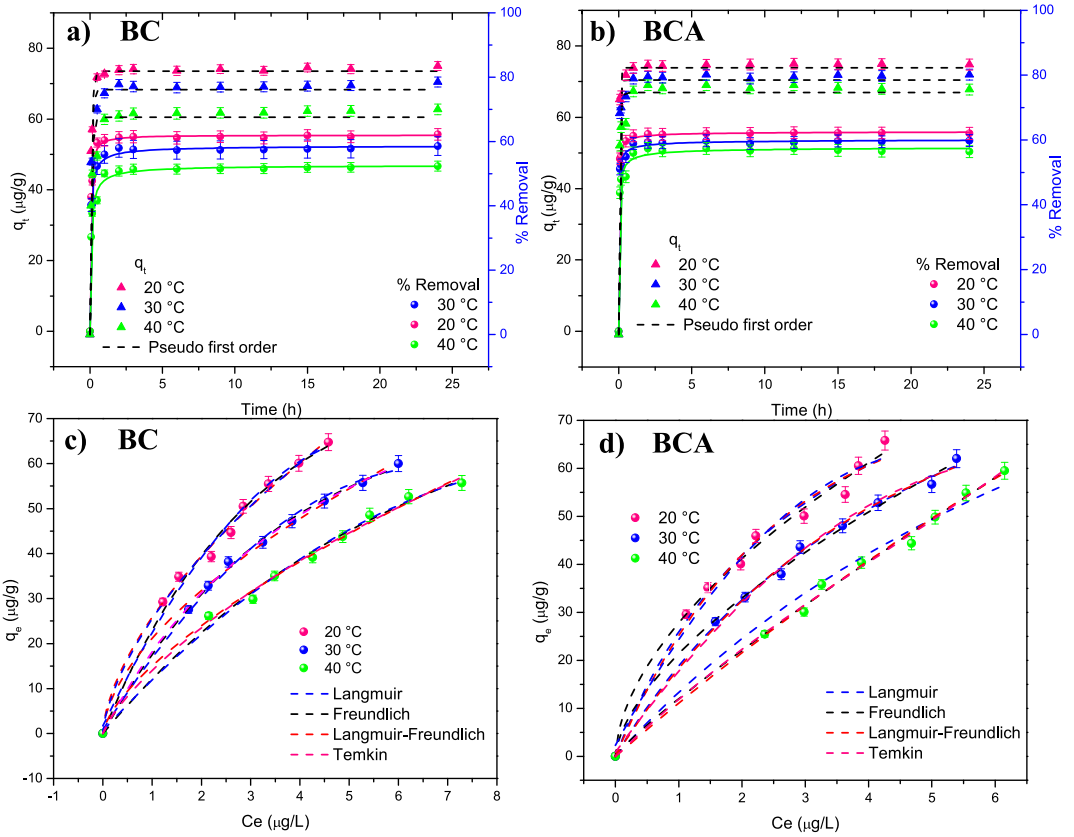

Fig. 2. Adsorption kinetics of (a) BC and (b) BCA, and adsorption isotherms of (c) BC and (d) BCA at 20, 30, and 40 °C.

deionized water, dried at 35 °C for 48 h, and subsequently subjected to pyrolysis, producing biochar (BC). For the chemically activated biochar (BCA), a portion of the ground seeds was treated with 0.5 M HNO_3 (Fermont®) prior to pyrolysis. Both BC and BCA were pyrolyzed at 650 °C for 3 h.

2.1.1. Characterization of BC and BCA

The morphology of BC and BCA was analyzed using a JEOL® JSM 5900 LV scanning electron microscope (SEM). Elemental composition was assessed via Energy-Dispersive X-ray Spectroscopy (EDS) in five different regions of each sample under vacuum conditions, using an OXFORD® INCAx-Act 51-ADD0013 probe.

Surface area, pore volume, and pore size distribution were determined using nitrogen adsorption isotherms on a Belsorp® Max III instrument. The density of active sites (σ) was evaluated through potentiometric titration with KOH, and the isoelectric point was determined by suspending different masses (0.05–1.25 g) of each material in 10 mL of deionized water at 25 °C, followed by pH measurement using a HANNA Instruments® HI8915 potentiometer after 24 h of agitation.

The energy states of the materials were analyzed using X-ray Photoelectron Spectroscopy (XPS) on a Thermo Scientific K-Alpha XPS® equipped with an Al monochromatic source (400 μm analysis diameter). A UV–Visible spectrophotometer (Thermo Scientific™ INSIGHT™) was used to obtain the absorption spectra of BC and BCA, and the bandgap was calculated using the Kubelka-Munk equation [25].

2.2. ZEN removal studies

2.2.1. Preparation and quantification of ZEN solutions

ZEN stock solutions were prepared using a ZEN CHIRON AS™ standard (initial concentration of 50 μg L^{-1}). ZEN concentrations were determined by UV–Vis spectrophotometry at 257 nm, using a PerkinElmer® Lambda 35 UV–Vis spectrophotometer.

2.2.2. Adsorption: kinetics and isotherm analysis

Batch adsorption experiments were conducted to evaluate ZEN adsorption kinetics. Polyethylene tubes containing 1.5 mg of BC or BCA were filled with a 520 μg L^{-1} ZEN solution, and samples were agitated at various contact times (5, 10, 30 min, and 1, 2, 3, 6, 9, 12, 15, 18, 24 h) at temperatures of 20, 30, and 40 °C (pH = 7). The kinetic data were analyzed using pseudo-first-order, pseudo-second-order, Elovich, and intraparticle diffusion models.

Table 1
Kinetics and adsorption isotherms of ZEN using BC and BCA.

		Adsoption kinetics					
		BC			BCA		
T (°C)		20	30	40	20	30	40
Pseudo first order	K_L (min^{-1})	12.64	11.98	10.76	23.19	22.25	22.22
	q_e ($\mu g\ g^{-1}$)	53.21	50.81	45.71	54.91	52.33	52.34
	R^2	**0.99**	**0.978**	**0.988**	**0.989**	**0.987**	**0.989**
Pseudo second order	K ($g\ \mu g^{-1} min^{-1}$)	5.33E+45	1.89E+45	6.33E+44	3.01E+43	1.32E+42	−2.76E+44
	q_e ($\mu g\ g^{-1}$)	52.35	48.46	43.95	54.16	51.54	51.56
	R^2	0.862	0.827	0.875	0.97	0.961	0.961
Elovich	A ($\mu g\ g^{-1} min^{-1}$)	5.28E+09	8.98E+08	5.95E+07	7.74E+18	2.91E+16	2.84E+16
	B ($g\ \mu g^{-1}$)	0.51	0.39	0.37	0.82	0.74	0.74
	R^2	0.961	0.95	0.953	0.971	0.972	0.969
Intraparticle diffusion	K ($\mu g\ g^{-1} min^{-1/2}$)	1.6	1.57	1.26	1.31	1.31	1.3
	C	42.72	39.22	33.17	45.43	43	40.01
	R^2	0.095	0.111	0.075	0.037	0.051	0.05
	Adsorption isotherms						
			BC			BCA	
T (°C)	20	30	40	20	30	40	
Langmuir	q_m ($\mu g\ g^{-1}$)	47.36	44.45	41.35	47.71	45.28	42.53
	K_L ($L\ \mu^{-1}$)	−1.8E+45	2.7E+45	1.5E+45	6.1E+45	−5.2E+44	−4.3E+45
	R_L	−2.7E-47	1.8E-47	3.1E-47	8.0E-48	−9.5E-47	−1.1E-47
	R^2	0.595	0.615	0.606	0.599	0.601	0.563
Freundlich	K_F ($\mu g\ g^{-1}$) ($L\ \mu g^{-1}$)$^{1/n}$	25.8	21.15	15.03	27.78	21.37	11.97
	N	0.61	0.59	0.68	0.57	0.63	0.88
	R^2	**0.994**	**0.997**	**0.993**	**0.99**	**0.996**	**0.995**
Langmuir/Freundlich	q_{MLF}	8782.7	8022.09	7045.21	9228.56	8146.25	6037.73
	k_{LF} ($L\ \mu g^{-1}$)	0.05	0.05	0.04	0.05	0.05	0.04
	MLF	0.3	0.29	0.33	0.28	0.31	0.44
	R^2	0.987	0.996	0.987	0.983	0.993	0.991
Temkin	q_m ($\mu g\ g^{-1}$)	90.13	95.19	92.87	96.3	89.52	69.03
	K_T ($\mu g\ L^{-1}$)	2.24	1.68	1.12	2.69	1.67	0.82
	R^2	0.993	0.996	0.992	0.988	0.994	0.993

To investigate adsorption isotherms, polyethylene tubes containing 1.5 mg of BC or BCA were filled with ZEN solutions at concentrations of 10–24 μg L^{-1} and agitated for 24 h at 20, 30, and 40 °C. The results were analyzed using Langmuir, Freundlich, Langmuir-Freundlich, and Temkin models. The effect of pH (range 2–12) on adsorption was also studied, with ZEN concentrations of 20 μg L^{-1} at the same temperature range. After agitation, ZEN concentrations were measured by UV–Vis spectrophotometry.

2.2.3. Photodegradation: kinetics and isotherm analysis

ZEN photodegradation kinetics were evaluated using a batch reactor containing 15 mg of BC or BCA and 50 mL of ZEN solution at concentrations of 20 μg L^{-1} (for $\lambda = 254$ nm) and 40 μg L^{-1} (for $\lambda = 365$ nm). Samples were stirred in the dark for 3 h to reach adsorption equilibrium, followed by UV irradiation at temperatures of 20, 30, and 40 °C (pH = 7). Aliquots (3 mL) were collected every 10 min (9 samples total), filtered through 0.45 μm Millipore® nitrocellulose filters, and analyzed to determine ZEN concentrations in the supernatant. Kinetic data were fitted to zero-order, first-order, second-order, and exponential decay models.

The effect of ZEN concentration was assessed at 20, 30, 40, and 50 μg L^{-1} using similar experimental conditions. Additionally, pH effects were studied in a range of 2–12 with ZEN concentrations of 20 μg L^{-1} ($\lambda = 254$ nm) and 40 μg L^{-1} ($\lambda = 365$ nm), with ZEN quantification conducted via UV–Vis spectrophotometry.

2.3. Regeneration and reuse studies

The reusability of BC and BCA in adsorption was assessed by performing desorption in an acidic medium (pH = 2) with 0.1 M HNO_3. After desorption, the materials were reused in adsorption experiments with ZEN solutions (20 μg L^{-1}, 20 °C, pH = 7) until the adsorption efficiency dropped significantly. Similarly, the photodegradation capacity of the materials was evaluated by cycling the process, using 15 mg of BC or BCA in a continuous flow reactor with ZEN solutions (20 μg L^{-1} at $\lambda = 254$ nm, 40 μg L^{-1} at $\lambda = 365$ nm).

2.4. Thermodynamic parameters and activation energy

Thermodynamic parameters, including Gibbs free energy (ΔG°), enthalpy (ΔH°), and entropy (ΔS°), were calculated using the integrated Van't Hoff equation [26] to examine temperature-dependent equilibrium data. The activation energy for both adsorption and photodegradation processes was also determined.

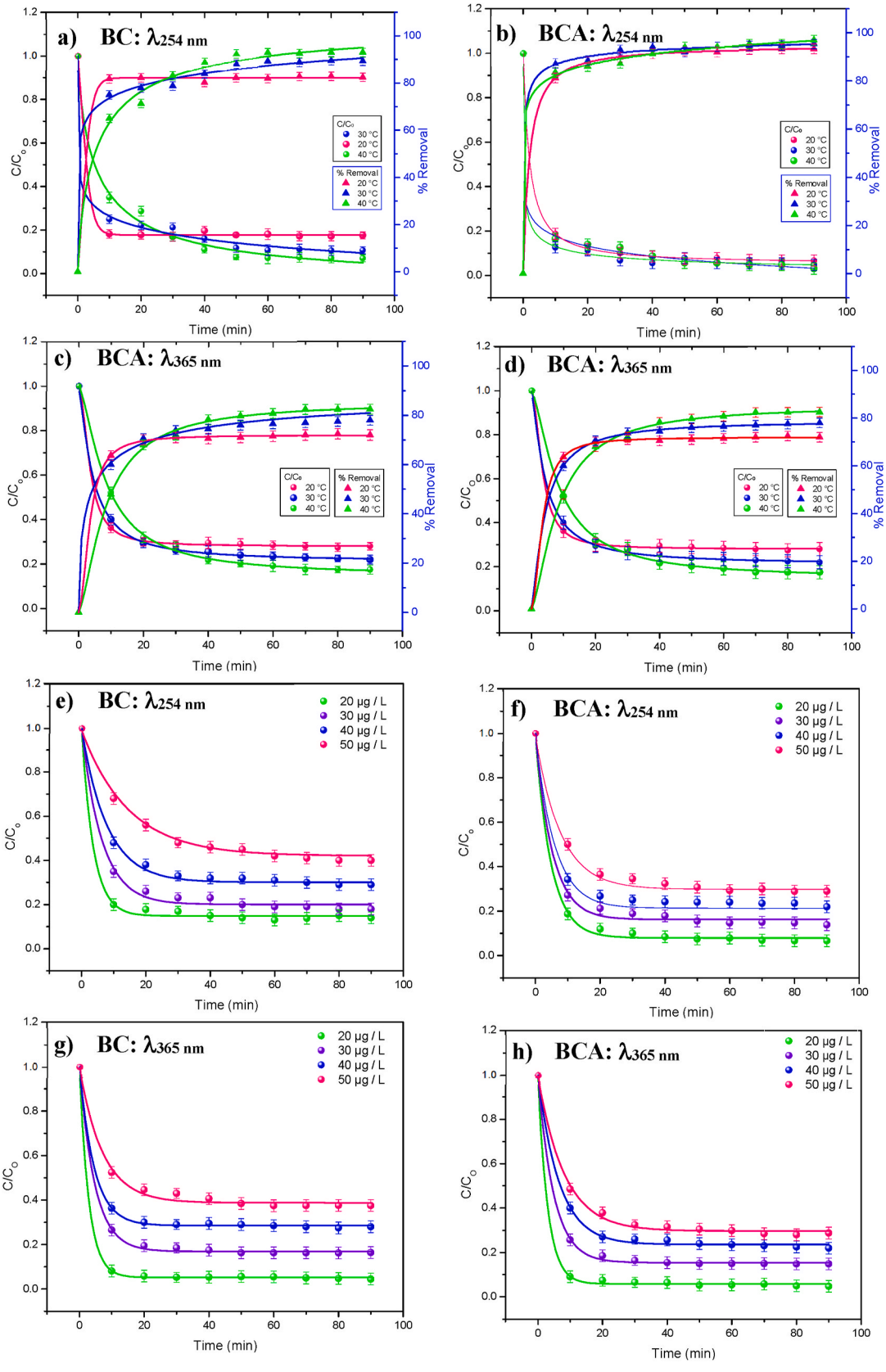

(caption on next page)

Fig. 3. Photodegradation kinetics at 20, 30, and 40 °C for (a) BC and (b) BCA at λ = 254 nm, and for (c) BC and (d) BCA at λ = 365 nm. Photodegradation as a function of initial concentration for (e) BC and (f) BCA at λ = 254 nm; and (g) BC and (h) BCA at λ = 365 nm.

$$Ln\,k = -\Delta^{\circ}H/R*1/\,T^{\circ} + \Delta S^{\circ}/R \quad \text{(Eq. 1)}$$

In this context, the variables are defined as follows: R is the ideal gas constant (J mol^{-1} K^{-1}), T represents the absolute temperature in Kelvin (K), and k is the constant derived from fitting the isotherm models.

Once the kinetics data were obtained, the reaction rate constant at 20, 30, and 40 °C were calculated. To explore the temperature dependence of the reaction, a plot of the natural logarithm of the rate constant (Ln k) versus the inverse of the absolute temperature (T^{-1}) in Kelvin was generated. This plot illustrates the relationship between temperature and reaction rate. The linear form of the Arrhenius equation [27] was then used (Eq. (2)) to determine the activation energy (Ea) and the pre-exponential factor (A).

$$Ln\,k = Ea/R\,(1\,/\,T^{\circ}) + Ln\,A \quad \text{(Eq. 2)}$$

In the equation provided, k represents the rate constant of the reaction at a specific temperature. Ea is the activation energy required for the process. The value of R is 8.314 kJ mol^{-1}, T denotes the temperature in Kelvin, and A is the frequency factor for the reaction.

3. Results and discussion

3.1. Structural features and surface characteristics

Fig. 1 illustrates the micrographs of BC and BCA before and after the adsorption of ZEN under controlled conditions (T = 20 °C, pH = 7, t = 24 h). The micrograph of BC prior to adsorption (Fig. 1a) reveals hexagonal and pentagonal cavities with an average diameter of 35 ± 0.5 μm, accompanied by minor folds in the cavity walls. EDS analysis confirms the presence of C (80.85 ± 5.34 %), O (3.06 ± 0.67 %), N (16.03 ± 1.56 %), and Ca (0.06 ± 0.02 %). Following adsorption (Fig. 1b), the overall morphology remains largely unchanged; however, EDS data show an increase in C (85.44 ± 3.34 %) and O (4.8 ± 0.34 %) content, with a corresponding decrease in N (9.73 ± 1.34 %) and Ca (0.03 ± 0.01 %). The observed increase in C and O suggests significant chemical interactions between the adsorbent and ZEN, likely driven by the element-rich nature of ZEN. In contrast, BCA (Fig. 1c) exhibits hexagonal cavities with diameters ranging from 25 ± 0.5 μm to 30 ± 0.5 μm. EDS analysis identifies C (84.33 ± 4.24 %), O (3.95 ± 0.94 %), N (11.66 ± 1.05 %), Ca (0.02 ± 0.01 %), and Na (0.04 ± 0.01 %), showing higher levels of C and O compared to BC. Post-adsorption (Fig. 1d), slight deformations in the hexagonal cavities are observed, along with the appearance of small particles on the cavity walls. EDS results indicate increased levels of C (86.1 ± 5.14 %), O (4.8 ± 0.98 %), N (9.01 ± 1.32 %), Ca (0.05 ± 0.02 %), and Na (0.04 ± 0.01 %), suggesting stronger interactions between ZEN and BCA. These findings indicate that both BC and BCA largely retain their morphology after adsorption, though BCA exhibits more pronounced surface modifications. The increase in C and O content for both materials confirms substantial chemical interactions between ZEN and the adsorbents. The surface changes observed in BCA can be attributed to a combination of physical and chemical interactions with ZEN. These observations underscore the critical role of the morphological features and composition of the materials in the adsorption process. The superior adsorption capacity of BCA compared to BC can be attributed to its enhanced structural and compositional properties. Similarities with biochars derived from other sources, such as pineapple peels [28], coconut residues [29], rice husks [30], sugarcane bagasse, orange peels, and peanut shells, highlight the potential of biochar materials for environmental applications. Such biochars provide valuable insights for designing and optimizing efficient adsorbents for contaminant removal.

Regarding surface properties, BC exhibits a higher specific surface area (55.60 m^2 g^{-1}) and pore volume (0.041 cm^3 g^{-1}) compared to BCA (14.9 m^2 g^{-1} and 0.019 cm^3 g^{-1}). These findings align with those reported by Fernando et al. [31], who observed similar results when employing HNO_3 as a pretreatment for the preparation of biochar derived from *Lasia spinosa*. The superior values observed for BC are attributed to the ability of HNO_3 to minimize the chemical decomposition of cellulose and hemicellulose during pyrolysis. Wang et al. [32], also emphasized that acid pretreatment of biomass can modify the surface morphology of biochars, promoting the formation of micro- and mesopores, enhancing crystallinity, and reducing inorganic components such as alkali and alkaline earth metals. Compared to other biochars, both BC and BCA display relatively large specific surface areas and pore diameters (2.98 and 5.27 nm, respectively). Reported values for other biochars include 7.2 m^2 g^{-1} [33], 45.29 m^2 g^{-1} [34], 6.60 m^2 g^{-1} [35], and 0.58 m^2 g^{-1} [36]. According to IUPAC classification [37], the biochars are mesoporous (>2 nm), which provides an advantage by facilitating increased surface contact between BC, BCA, and ZEN, thereby improving both adsorption and photocatalytic processes.

An analysis of active sites as a function of specific surface area (Ae) reveals an increase from 3 sites nm^{-2} for BC to 6 sites nm^{-2} for BCA. Additionally, BC exhibits an isoelectric point (IP) at pH = 7 ± 0.3, whereas BCA has an IP at pH = 8 ± 0.3. This suggests that the BC surface undergoes hydroxylation (OH^-) at pH levels above the IP and protonation (H^+) at pH levels below this value [38,39].

3.2. Band gap determination

In this study, the bandgap of each material was determined through the analysis of diffuse reflectance spectra using the Kubelka-Munk method [25]. The results revealed bandgap values of 1.6 eV for BC and 1.8 eV for BCA, which are consistent with values reported in previous studies [40]. Notably, biochars typically exhibit lower bandgap values compared to other materials, a characteristic attributed to their porous structure [41].

Table 2
Kinetic modeling of ZEN photodegradation using BC and BCA.

		λ (254 nm)						λ (365 nm)					
		BC			BCA			BC			BCA		
T (°C)		20	30	40	20	30	40	20	30	40	20	30	40
Zero order	K ($\mu g \cdot L^{-1}$ min^{-1})	0.01	0.01	0.01	0.01	0.01	0.01	0.01	0.01	0.01	0.01	0.01	0.01
	R^2	0.14	0.11	0.1	0.15	0.16	0.14	0.05	0.1	0.08	0.11	0.06	0.1
First order	K (min^{-1})	0.07	0.08	0.11	0.11	0.14	0.18	0.03	0.03	0.03	0.03	0.04	0.04
	R^2	0.62	0.81	0.93	0.93	0.95	0.94	0.25	0.54	0.82	0.82	0.74	0.89
Second order	Kc ($L.\ \mu g\ min^{-1}$)	0.16	0.17	0.18	0.34	0.36	0.48	0.07	0.08	0.08	0.08	0.09	0.1
	R^2	0.85	0.96	0.98	0.98	0.97	0.98	0.71	0.87	0.98	0.98	0.96	0.98
Exp. decay	k (min^{-1})	0.11	0.15	0.18	0.2	0.22	0.26	0.08	0.14	0.2	0.13	0.24	0.28
	α	1	0.99	0.98	0.99	0.99	0.99	0.99	0.99	0.99	0.99	0.99	0.99
	C_r ($\mu g\ L^{-1}$)	0.17	0.13	0.08	0.08	0.06	0.07	0.28	0.23	0.18	0.18	0.19	0.13
	R^2	0.99	0.98	0.99	0.99	0.99	0.99	0.99	0.99	0.99	0.99	0.99	0.99

3.3. Adsorption process

3.3.1. Kinetic study and isotherms: effect of pH variation and concentration

The analysis of the adsorption kinetics provides key insights into the performance of BC and BCA materials in the removal of ZEN from aqueous media. Fig. 2a and b demonstrate that the initial phase of adsorption occurs rapidly due to the abundance of active sites within the mesoporous structure of the biochar. However, as equilibrium is reached (after 3 h), most of these sites become occupied, leading to a decrease in the adsorption rate [42]. This behavior indicates a rapid initial adsorption phase, followed by a slower equilibrium phase.

Regarding removal efficiency, the BC material exhibited high adsorption percentages: 82 % at 20 °C, 79 % at 30 °C, and 70 % at 40 °C, with adsorption capacities of 55.66 μg g^{-1}, 52.33 μg g^{-1}, and 46.66 μg g^{-1} of ZEN, respectively. In contrast, the BCA material showed slightly higher removal efficiency, with values of 84 % at 20 °C, 80 % at 30 °C, and 75 % at 40 °C, reaching capacities of 57.5 μg g^{-1}, 53.01 μg g^{-1}, and 50.36 μg g^{-1}, respectively. These results suggest that chemical treatment improves the adsorption properties of BCA, likely due to enhanced surface functionalization.

Although studies on the adsorption of ZEN onto carbonaceous materials are limited, previous research on the removal of mycotoxins using carbon-based materials provides valuable insights. For instance, one study utilized biochar derived from soybean residues to remove deoxynivalenol, achieving an efficiency of 88 % (52.98 μg g^{-1}) within just 10 min of contact [43]. Similarly, an adsorption efficiency of 79 % (0.27 μg g^{-1}) for ochratoxin A was reported within 30 min using biochar derived from walnut shells [13]. These findings, along with those of the current study, underscore the effectiveness of biochars in removing mycotoxins within the initial minutes of interaction.

At 20 °C, adsorption capacity is favored, likely because the ZEN molecules possess sufficient thermal energy to overcome the activation barrier and adsorb effectively onto the surface of the biochar [44]. However, as temperature increases, the kinetic energy of the ZEN molecules rises, which may reduce adsorption effectiveness by decreasing molecular interactions with the adsorbent surface [45]. This behavior is characteristic of exothermic processes, where adsorption capacity decreases with rising temperature, as also observed in other organic contaminants. A similar adsorption behavior was observed for metronidazole and tetracycline using biochar derived from rice bran, where adsorption efficiency decreased at temperatures above 20 °C [46].

On the other hand, Fig. 2c and d demonstrate the ability of BC and BCA to efficiently and consistently adsorb ZEN at varying concentrations. These figures also highlight the adverse effect of temperatures above 20 °C on the adsorption capacity, an aspect that must be carefully considered in practical applications of water treatment for mycotoxins such as ZEN. A consistent linear relationship is observed between the ZEN concentration and the amount adsorbed onto both BC and BCA, indicating that the adsorption sites on both materials remain accessible across the concentration range studied [47]. The experimental data were well-fitted to the Pseudo-First Order kinetic model, with correlation coefficients (R^2) close to 1 (Table 1), suggesting that physisorption is the predominant process for both materials (Eq. (3)). This model also provides information on the adsorption rate constant (K_L), which tends to decrease with increasing temperature, reflecting the speed at which adsorption equilibrium is reached [48].

$$q_t = q_e\left(1 - e^{(-k_L t)}\right) \quad \text{(Eq. 3)}$$

Where q_t and q_e are the equilibrium concentrations of adsorbed ZEN at a given time, respectively (μg g^{-1}), and K_L is the adsorption rate constant (g mg^{-1} min^{-1}). As a result of the mathematical fittings, it is observed that the values of q_t decrease as temperature increases, ranging from 53 ± 0.3 μg g^{-1} to 45 ± 0.3 μg g^{-1} for BC, while for BCA, the values are slightly higher: 55 ± 0.3 μg g^{-1} and 52 ± 0.3 μg g^{-1}, respectively. This behavior could be attributed to weaker van der Waals forces between the active sites of the adsorbent and the adsorbate molecules [49]. The rate constants (k) also gradually decrease with increasing temperature, confirming that the adsorption equilibrium is reached more quickly at 20 °C. Additionally, the constants β and α, related to chemisorption and surface characteristics, suggest higher adsorption rates, particularly for BC, where a lower β value indicates greater efficiency in ZEN adsorption. However, this study suggests that both BC and BCA are effective for adsorbing organic contaminants, with BCA showing a slight advantage where temperature plays a crucial role, as better adsorption is observed at lower temperatures due to stronger physical interactions between

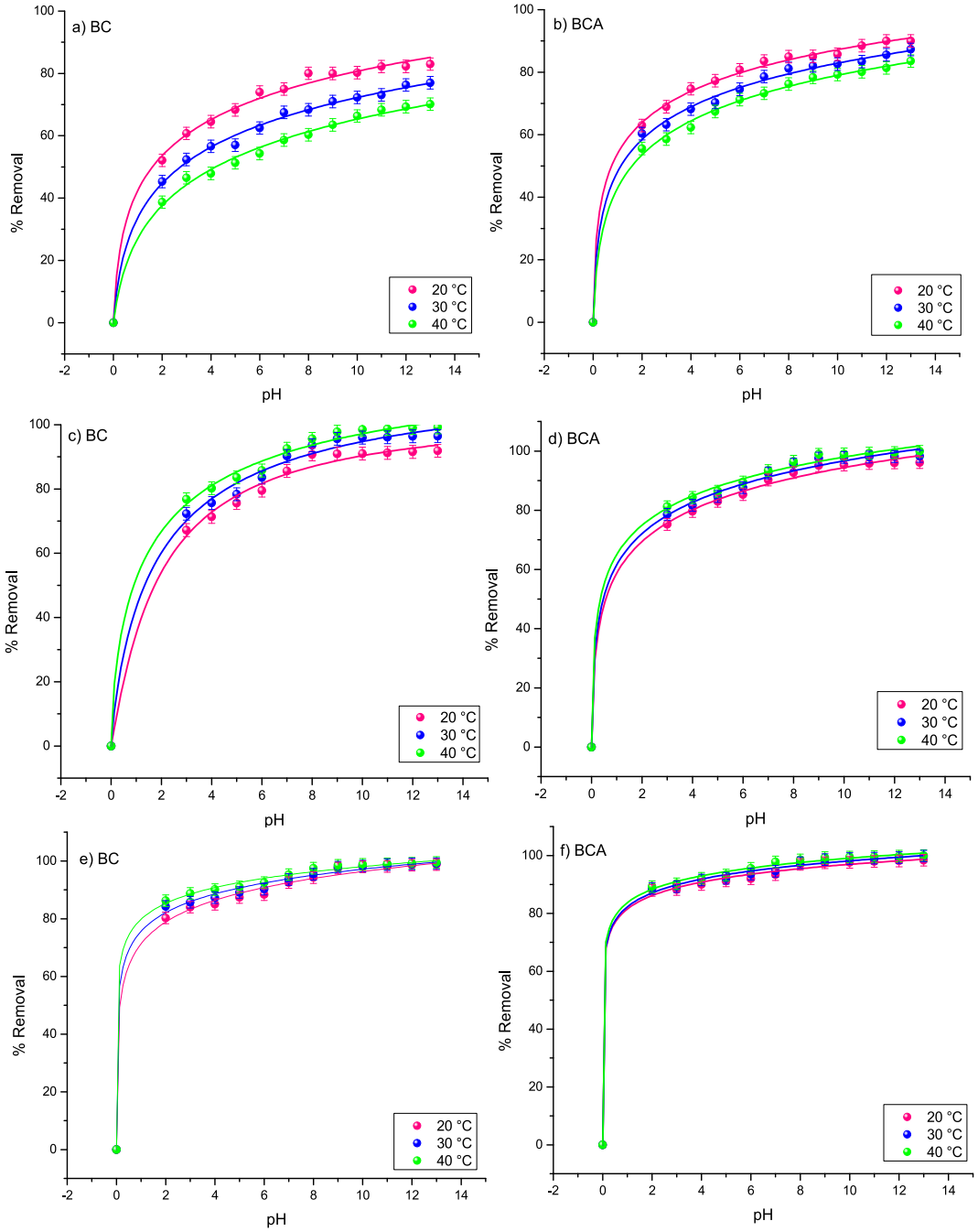

Fig. 4. Effect of pH on ZEN removal: (a) BC and (b) BCA for adsorption; (c) BC and (d) BCA for photodegradation at λ = 254 nm; and (e) BC and (f) BCA for photodegradation at λ = 365 nm.

the adsorbent and adsorbate.

The Freundlich model demonstrates a superior fit to the experimental adsorption isotherm data for both BC and BCA, as evidenced by correlation coefficients close to 1 (Table 1). This observation aligns with findings for ZEN adsorption on activated carbon [50], indicating a non-ideal and heterogeneous adsorption pattern on the material surface. The Freundlich parameter *n*, which reflects adsorption intensity, is less than 1 for both materials, suggesting weak adsorption predominantly, governed by physisorption. In this context, the interactions between ZEN and the active sites on BC and BCA are primarily physical in nature [51].

Nevertheless, the possibility that chemisorption may also occur cannot be entirely ruled out, as both the Freundlich and Temkin models show similar correlation coefficients. This implies that, although physisorption is the dominant mechanism, some degree of chemisorption could simultaneously occur, albeit to a lesser extent.

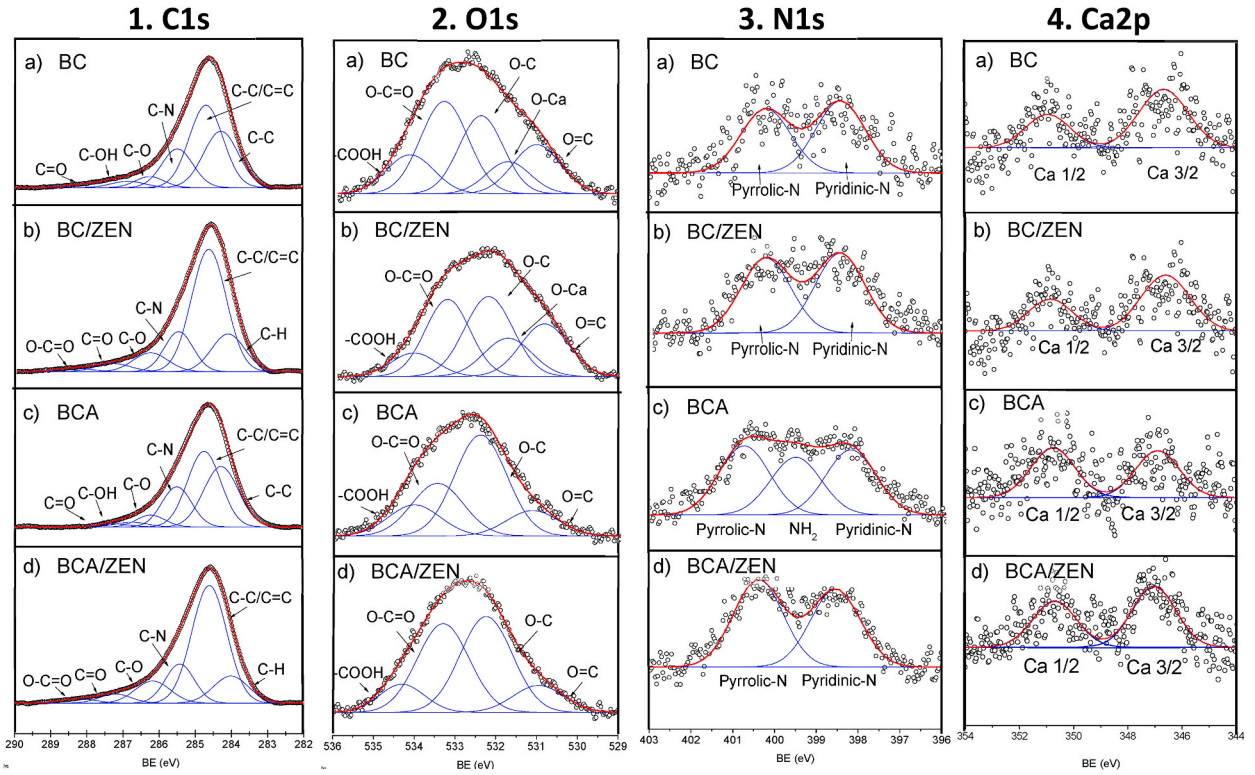

Fig. 5. Deconvolution of 1) C1s, 2) O1s, 3) N1s, and 4) Ca2p spectra before and after adsorption on BC and BCA respectively.

3.3.2. Photodegradation process

In the photocatalysis process, ZEN degradation is observed to be more effective at a wavelength of $\lambda = 254$ nm and temperatures above 20 °C. BCA demonstrates superior efficiency compared to BC, achieving degradation rates of 93 % (18.6 μg L^{-1}), 95 % (19 μg L^{-1}), and 97 % (19.4 μg L^{-1}) at 20, 30, and 40 °C, respectively. In contrast, BC achieves only 82 % (16.4 μg L^{-1}), 89 % (17.8 μg L^{-1}), and 92 % (18.4 μg L^{-1}) under the same conditions (Fig. 3a and b). These findings suggest that the acid pretreatment of BCA results in a higher density of hydroxyl groups, enhancing ZEN degradation by increasing surface activity [52]. Both materials reach equilibrium in the photocatalysis process within 60 min, indicating a rapid initial reaction followed by a stable phase.

Fig. 3c and d depict the degradation of ZEN at $\lambda = 365$ with an initial concentration of 40 μg L^{-1}, where both materials achieve photodegradation efficiencies exceeding 97 % within the initial minutes. These results are comparable to those previously reported using graphite [53], which demonstrated photodegradation efficiencies of 95 % (475 μg L^{-1}) and 97 % (485 μg L^{-1}) at wavelengths of 254 nm and 365 nm, respectively, reaching equilibrium within 50 min. It is observed that as the temperature increases, the degradation efficiency also improves, albeit to a lesser extent than at $\lambda = 254$ nm. For BC, the degradation percentages were 72 % (14.4 μg L^{-1}), 78 % (15.6 μg L^{-1}), and 82 % (16.4 μg L^{-1}) at 20, 30, and 40 °C, respectively. Similarly, for BCA, the degradation percentages were 74 % (14.8 μg L^{-1}), 79 % (15.8 μg L^{-1}), and 85 % (17 μg L^{-1}).

These results indicate that both BC and BCA are effective for ZEN degradation, particularly at temperatures >20 °C and under suitable wavelengths to activate the process. Higher temperatures promote e^-/h^+ recombination, thereby enhancing process efficiency [54,55]. Additionally, the effect of initial concentration on photocatalysis (Fig. 3e–h) at $\lambda = 254$ and 365 nm shows that equilibrium is rapidly reached within the first 40 min, regardless of ZEN's initial concentration. This rapid degradation onset highlights the high photocatalytic activity of BC and BCA under UV light irradiation. Notably, at $\lambda = 365$ nm, ZEN degradation reaches 97 % from an initial concentration of 20 μg L^{-1}, showcasing superior performance compared to $\lambda = 254$ nm. This suggests that the UV wavelength significantly impacts photocatalytic efficiency, likely due to greater energy absorption by BC and BCA photocatalysts at $\lambda = 365$ nm [56].

The experimental data for the photodegradation of Zearalenone (ZEN) using BC and BCA were fitted to mathematical models (Table 2), showing that the exponential decay model provided the best fit for both materials at wavelengths of 254 and 365 nm. This model assumes that the reaction rate is influenced not only by the ZEN concentration but also by the availability of active sites on the BC and BCA surfaces [57,58]. These results confirm the effectiveness of the photodegradation process and the ability of both materials to efficiently remove ZEN from aqueous media. BCA exhibited a higher degradation rate compared to BC at both wavelengths. At $\lambda = 254$ nm, the reaction rate constants for BC ranged from 0.11 to 0.18 min^{-1}, whereas BCA demonstrated superior values between 0.20 and 0.26 min^{-1}. Similarly, at $\lambda = 365$ nm, BC showed rate constants ranging from 0.08 to 0.22 min^{-1}, while BCA achieved values between 0.13 and 0.28 min^{-1}. These results suggest that BCA facilitates a faster photocatalytic process for ZEN, likely due to its higher

Table 3
Energetic States of C1s, O1s, N1s, and Ca2p in BC and BCA before and after ZEN adsorption.

		BC						BCA					
		Before			*After*			*Before*			*After*		
	Energy states	**BE (eV)**	**FWHM**	**Area**	**BE (eV)**	**FWHM**	**Area**	**BE (eV)**	**FWHM**	**Area**	**BE (eV)**	**FWHM**	**Area**
C1s	**O-C = O**	–	–	–	288.4	1.14	1.62	–	–	–	288.3	1.14	2.08
	C = O	287.3	1.14	1.49	287.3	1.14	3.68	287.3	1.05	1.49	287.3	1.02	3.89
	C-OH	286.7	1.14	2.42	–	–	–	286.7	1.05	2.42	–	–	–
	C-O	286.3	1.1	5.34	286.3	1.14	8.5	286.3	0.94	5.34	286.2	1.14	10.45
	C-N	285.6	1.14	18.63	285.5	0.94	14.85	285.6	1.14	18.63	285.5	0.94	15.22
	C-C/C = C	284.7	1.1	39.3	284.6	1.14	55.09	284.7	1.14	42.9	284.7	1.14	55.54
	C-C	284.3	1.14	32.79	–	–	–	284.2	1.14	32.79	–	–	–
	C-H	–	–	–	284	1.08	16.23	–	–	–	284	1.14	12.79
O1s	**COOH**	534.2	1.4	13.8	534.1	1.31	8.37	534.1	1.5	14.78	534.2	1.46	10.33
	O-C = O	533.4	1.4	32.63	533.3	1.3	27.04	533.4	1.5	25.03	533.3	1.5	37.73
	O-C	532.4	1.3	25.63	532.3	1.4	30.18	532.4	1.5	40.8	532.3	1.5	42.5
	O-Ca	531.7	1.3	10.55	531.7	1.4	14.48	–	–	–	–	–	–
	O = C	531	1.4	17.37	531	1.4	19.9	531.1	1.5	2.11	531	1.3	11.13
N1s	**N = C**	400.2	1.4	47.93	400.4	1.4	48.42	400.5	1.4	36.04	400.4	1.4	52.97
	N-H	–	–	–	–	–	–	399.6	1.4	30.05	–	–	–
	N-C	398.4	1.4	52.06	398.4	1.4	51.57	398.2	1.4	33.9	398.5	1.4	40.8
Ca2p	**Ca2p 1/2**	351.2	1.7	33.93	351.18	1.7	33.73	351.3	1.9	51.58	350.98	1.9	43.05
	Ca2p 3/2	347.4	1.9	66.06	347.36	1.9	66.26	347.4	1.9	48.41	347.03	1.9	56.95

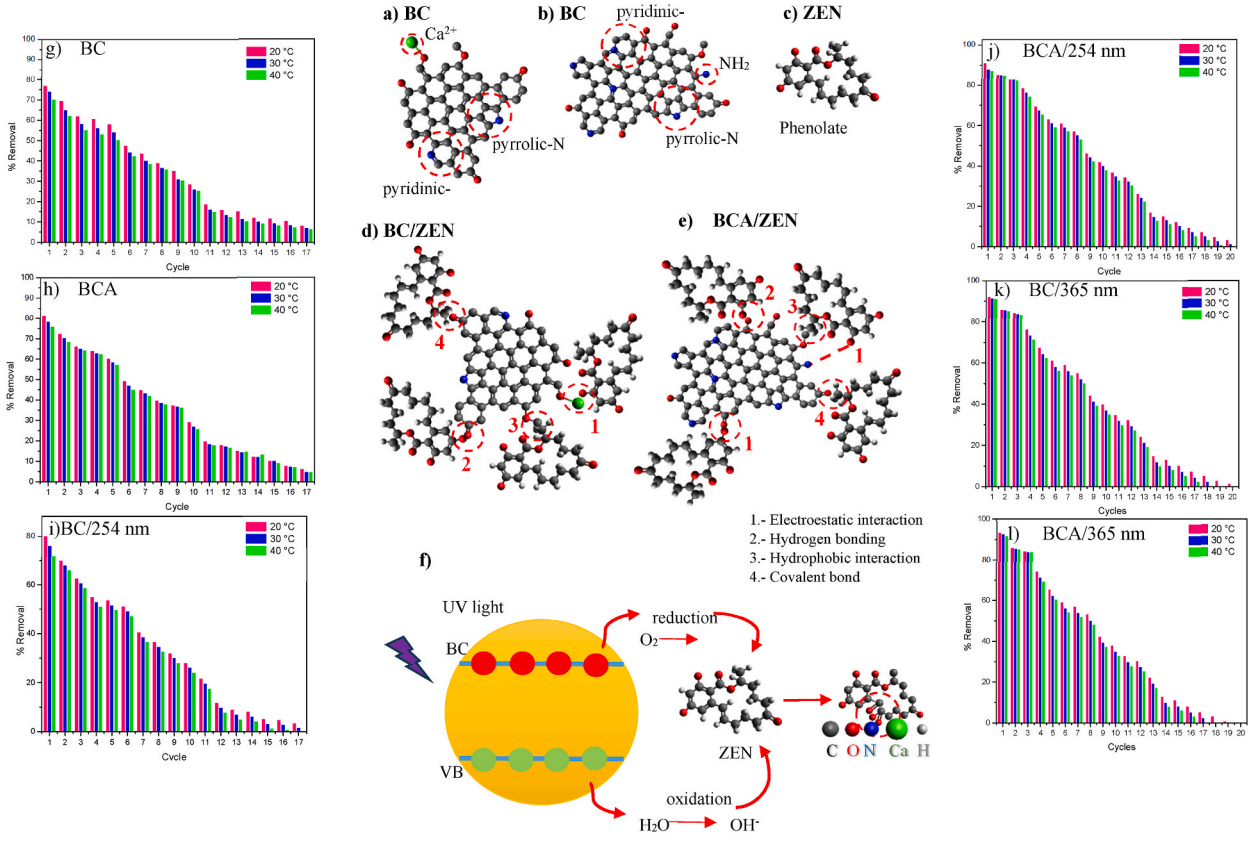

Fig. 6. Proposed structure of a) BC, b) BCA, c) anionic form of ZEN, d) adsorption on BC, and e) BCA, f) ZEN photodegradation mechanism. Reuse cycles in adsorption with g) BC and h) BCA, photodegradation of i) BC and j) BCA at λ = 254 nm, and k) BC and l) BCA at λ = 365 nm.

density of active functional groups and the enhanced generation of OH^- radicals during the photocatalytic reaction. Additionally, an increase in reaction temperature was observed to improve the ZEN degradation rate. Higher temperatures enhance charge carrier mobility and charge transport at the interface, leading to increased collision frequency between ZEN molecules or their degradation intermediates and the biochar surface. This promotes the generation of OH^- radicals and accelerates degradation [59].

3.4. Influence of pH on the adsorption and photocatalysis processes

Previous studies have shown that the adsorption of organic compounds onto carbonaceous materials can be significantly influenced by the solution pH [60,61]. Analysis of Fig. 4 reveals the relationship between system pH and the adsorption percentage of ZEN, demonstrating an increase in adsorption with rising pH. Maximum adsorption values of 83 % (16.6 μg L^{-1}) for BC and 90 % (18 μg L^{-1}) for BCA are achieved (Fig. 4a and b). This behavior can be attributed to the presence of active sites on the material surfaces and the pKa1 of ZEN, which is 3.62. At pH > 8, the presence of hydroxyl groups (OH^-) enhances both adsorption and photocatalysis processes by promoting the generation of free radicals that facilitate ZEN adsorption and degradation in aqueous media (Fig. 4c–f) [62]. The influence of pH is closely related to the isoelectric point (IEP) of the materials, which is approximately pH 7 ± 0.3 for BC and pH 8 ± 0.3 for BCA. This characteristic enables the materials to adsorb both positively and negatively charged ZEN species, depending on the pH of the medium. The distribution of ZEN species in solution varies with pH, significantly affecting the efficiency of both adsorption and photocatalysis by determining the specific interactions between the contaminant and the adsorbent surface. At pH < 7, ZEN predominantly exists in its non-ionized form [63], facilitating adsorption through hydrophobic and π–π interactions. In contrast, at pH > 7, ZEN may ionize, potentially increasing electrostatic repulsion if the adsorbent surface is also negatively charged, thereby reducing adsorption efficiency.

3.5. Activation energy and thermodynamic parameters

The adsorption and photocatalysis processes of Zearalenone (ZEN) on BC and BCA reveal key aspects that influence the efficiency of these materials for contaminant removal. The activation energy (Ea) values for adsorption on BC (8.75E-05 kJ mol^{-1}) and BCA (6.25E-05 kJ mol^{-1}), both below 40 kJ mol^{-1}, indicate that physisorption is the predominant mechanism. These low activation energies suggest that ZEN adsorption primarily occurs through van der Waals forces and other weak interactions, such as hydrogen bonds between the adsorbate and adsorbent [19]. Furthermore, the exothermic nature of the adsorption process is supported by the negative values of enthalpy (ΔH°) (BC = −20.5 and BCA = −32 kJ mol^{-1}) and Gibbs free energy (ΔG°), indicating that the process is spontaneous and energy-releasing [64].

On the other hand, the Ea values are higher for the photocatalysis process on BC (λ254 = 18.84 and λ365 = 35.05 kJ mol^{-1}) and BCA (λ254 = 9.97 and λ365 = 29.46 kJ mol^{-1}), suggesting a faster reaction rate during this stage, likely due to the increased recombination of e^-/h^+ pairs at higher temperatures [55]. The small variations in enthalpy (ΔH) for BC and BCA at both λ = 254 and λ = 365, coupled with relatively low values of ΔG, indicate that photocatalysis requires less energy compared to adsorption. This behavior is attributed to the generation of free radicals, such as hydroxyl radicals (•OH), during photocatalysis, which efficiently degrade ZEN under UV irradiation [65]. The negative entropy values (BC: λ254 = −0.04, λ365 = −0.09 J mol^{-1} K^{-1}; BCA: λ254 = −0.02, λ365 = −0.08 J mol^{-1} K^{-1}) suggest that during the photocatalysis process, the system experiences an increase in order, generally indicating more stable adsorption of the reaction products on the catalyst surface.

3.6. Determination of the energy states using XPS in BC and BCA

X-ray photoelectron spectroscopy (XPS) analysis provides valuable insights into the interactions between the material surfaces and Zearalenone (ZEN) during the adsorption process. Several energy states were identified, including C1s, O1s, N1s, Ca2p, and Na1s. The atomic percentages obtained were as follows: for BC, C (90.8 %), O (7.37 %), N (1.51 %), Ca (0.3 %), and Na (0.02 %); and for BCA, C (94.15 %), O (3.58 %), N (1.73 %), Ca (0.02 %), and Na (0.08 %). After the ZEN adsorption process, a significant increase in the carbon percentage was observed, suggesting a strong interaction with the adsorbate. For C1s (FWHM of 1.1 ± 0.1) (Fig. 5.1a and c), several Gaussian peaks were detected, representing different energy states such as C-C (phenolic), C-C/C=C (aromatic), C-N, C-OH, and C=O (carboxyl groups), both before and after adsorption [66,67]. After the adsorption process (Fig. 5.1b and d), two new Gaussian peaks emerged, indicating interactions with alkyl groups (C-H) and carboxyl groups present in ZEN (O-C=O) [68].

Regarding oxygen (O1s), four energy states were identified corresponding to O=C, O-C=O, O-C, and -COOH, both before (Fig. 5.2a and c) and after adsorption (FWHM of 1.4 ± 0.1) (Fig. 5.2b and d). The O=C group may play a crucial role as an electron acceptor in reactions, potentially promoting the degradation of ZEN. This is supported by the presence of free radicals on the surface of the carbon formed during the pyrolysis process [69]. For nitrogen (N1s) (FWHM of 1.4 ± 0.1), energy states such as N-C and N=C, associated with pyridinic and pyrrolic nitrogen, were observed before adsorption (Fig. 5.3a and c) [70,71]. In BCA, a new energy state attributed to NH_2 emerged, which may indicate strong interactions between ZEN and the material surface (Fig. 5.3b and d) [72]. Finally, the energy states of Ca2p in both materials before (Fig. 5.4a and c) and after (Fig. 5.4b and d) adsorption indicated the presence of $CaCO_3$, which may influence the surface properties of the materials and their adsorption capacity [73].

Table 3 presents the detailed results of the X-ray photoelectron spectroscopy (XPS) analysis, providing insights into the interactions between the functional groups of BC and BCA with Zearalenone (ZEN), and revealing how these interactions influence the adsorption processes. Prior to ZEN adsorption, the C1s spectra of both materials showed predominant peaks corresponding to C-C and C=C, indicating the presence of aromatic structures formed from the decomposition of cellulose. The slightly higher area of the C-C/C=C peak in BCA compared to BC suggests that BCA has a higher degree of aromatic condensation, likely due to treatment with HNO_3 during demineralization. This increased aromaticity in BCA may contribute to a higher adsorption capacity by providing more active sites for interaction with ZEN.

Significant changes in the C=O and C-O states in the C1s spectra were observed after ZEN adsorption. This suggests that ZEN interacts with the functional groups on the material surfaces, possibly forming chemical bonds. The appearance of these new peaks

Table 4
Comparison of ZEN adsorption capacity and photodegradation efficiency.

Material	Mycotoxin	Removal capacity (q_m)	% Removal	Process	Mass (mg)	T (°C)	Reference
OKR-50	ZEN	1.6 mg g^{-1}	57	Adsorption	10	20	[77]
NMMT	ZEN	1.9 mg g^{-1}	95		30	37	[83]
BZ-2	ZEN	2.64 mg g^{-1}	38		3	–	[47]
Montmorillonite	ZEN	0.2 mg g^{-1}	49		10	–	[84]
Activated carbon	ZEN	0.29 mg g^{-1}	83		30	–	[50]
Graphitic carbon nitride	ZEN	–	95	Photodegradation	20	–	[53]
Graphene/ZnO	Aflatoxin B1	–	99		25	–	[85]
Activated carbon	Deoxynivalenol	–	99		15	–	[86]
Graphene	Deoxynivalenol	–	87		20	–	[87]
BC	ZEN	25.8 μg g^{-1}	95	Adsorption/	1.5	20	This work
BCA		27.7 μg g^{-1}	97	Photodegradation			

indicates that the adsorption process involves not only physical interactions but also the formation of chemical bonds, which may enhance the efficiency of contaminant removal. This finding supports the hypothesis that chemical interactions, in addition to physical interactions through van der Waals forces, play a crucial role in ZEN adsorption, improving retention on the adsorbent surface. The O1s spectra show changes in energy values for COOH, C-O, and O-Ca after ZEN adsorption, indicating that these oxygen-containing groups participate in surface interactions with the contaminant. The involvement of these functional groups suggests that they play a key role in the adsorption process, possibly through hydrogen bonding or other surface interactions that stabilize ZEN on the adsorbent surface. Specifically, the COOH and C-O groups may facilitate stronger interactions, promoting more efficient adsorption.

In the case of N1s, no significant changes were observed in the nitrogen states in BC before and after adsorption. However, in BCA, a new Gaussian peak corresponding to NH_2 groups appeared after ZEN adsorption, indicating that the amino groups may play a crucial role in the adsorption process by forming stable interactions with the contaminant. Finally, in the Ca2p spectra, some Gaussians showed a shift in binding energy for both Ca 1/2 and Ca 3/2 states, suggesting that the Ca-O bond is involved in interactions with ZEN. This shift indicates that calcium-containing groups on the surface participate in the adsorption process, possibly enhancing the adsorption capacity of the contaminant by providing additional sites for interaction.

3.7. Proposed mechanisms of adsorption and photocatalysis of BC and BCA against ZEN

Fig. 6 provides an overview of the mechanisms underlying the adsorption and degradation of Zearalenone (ZEN) using BC (Fig. 6a) and BCA (Fig. 6b) at pH 7. At this pH, the predominant form of ZEN in solution is the phenolate anion (Fig. 6 c), which significantly influences its interaction with these adsorbent materials. The results indicate that ZEN adsorption is primarily governed by physisorption, with minor contributions from chemisorption. Physisorption is characterized by weak van der Waals forces and hydrogen bonds, whereas chemisorption involves the formation of stronger chemical bonds. This finding aligns with the literature, which suggests that physisorption is the dominant adsorption mechanism for ZEN on carbon-based materials [74]. In BC, O-Ca^+ groups interact electrostatically with the O^- groups of the ZEN phenolate anion (Fig. 6 d1), with this electrostatic attraction being key to the adsorption efficiency of the biocarbons [50]. In contrast, in BCA, -NH_2^+ groups facilitate adsorption through hydrogen bonds with the ZEN phenolate anion (Fig. 6e1) [75]. Additionally, hydrogen bonds between the O^- of ZEN and the O-H groups present on both BC and BCA also contribute significantly to the adsorption process (Fig. 6d2-e2) [76]. This highlights the important role of hydrogen interactions in stabilizing ZEN on the adsorbent surfaces.

Hydrophobic interactions are also significant, as the methyl groups of ZEN interact with the carbon surfaces of BC and BCA, generating C-C interactions that enhance adsorption [77] (Fig. 6d3-e3). Furthermore, covalent C-O bonds between the methyl groups of ZEN and oxygen atoms on the material surfaces are crucial for stabilizing the adsorption complexes (Fig. 6d4-e4). Regarding ZEN photodegradation (Fig. 6f), UV irradiation generates free radicals on the surfaces of the biocarbons. These absorb UV energy, generating electrons (e^-) in the conduction band (CB) and holes (h^+) in the valence band (VB). The excited electrons can reduce O_2 to form superoxide radicals (O_2^-), while the holes oxidize H_2O to generate hydroxyl radicals (OH^-). These highly reactive radicals play a central role in the breakdown of ZEN in aqueous media. The photocatalytic pathway involves the opening of the lactone ring of resorcinol in ZEN, leading to the formation of aldehydes at both ends of the double bond [53]. This process underscores the effectiveness of biocarbons as photocatalysts and highlights the complexity of the photochemical mechanisms involved in contaminant degradation.

3.8. Reuse cycles of the materials for adsorption and photocatalysis processes

To determine the reuse cycles of the materials, regeneration tests were conducted on BC and BCA for the adsorption and photocatalysis processes, respectively. For the adsorption process, the maximum ZEN removal capacity was evaluated at three different temperatures (20, 30, and 40 °C). The results showed that, in the case of BC, the adsorption efficiency progressively decreased from 77 % in the first cycle to 8 % in the 17th cycle (Fig. 6g). Similarly, for BCA, a decrease in removal capacity was observed, with an initial efficiency of 80 %, which dropped to 7 % in the last cycle (Fig. 6h). Although a gradual loss of efficiency was observed with increasing

cycles, both materials demonstrated reusability, maintaining their adsorptive capacity over multiple cycles, positioning both materials as viable alternatives for long-term applications.

Additionally, the regeneration capacity of the materials was evaluated in the photocatalysis of ZEN using two different wavelengths (254 and 365 nm). For $\lambda = 254$ nm, BC exhibited an initial removal of 79 % in the first cycle, which decreased to 5 % after 17 cycles (Fig. 6i), while BCA showed higher removal efficiency, initially 85 %, dropping to 3 % after 20 cycles (Fig. 6j). Under irradiation at $\lambda = 365$ nm, BC demonstrated significantly superior performance, with an initial removal of 90 %, decreasing to 3 % after 20 cycles (Fig. 6k), while BCA achieved an initial efficiency of 97 %, which decayed to 1 % after 19 cycles (Fig. 6l).

When compared to studies reported in the literature, where up to 70 % degradation was achieved after just five cycles using magnetic biochar [78], BC and BCA demonstrate remarkably high regeneration capacities. This highlights the superior durability of BC and BCA, particularly under photocatalytic conditions at $\lambda = 365$ nm. In contrast, other studies [79,80] have reported more rapid efficiency losses under UV irradiation, emphasizing the potential of BC and BCA as promising materials for prolonged applications in the adsorption and degradation of ZEN.

Table 4 presents a comparative analysis of the ZEN adsorption and photocatalysis efficiencies obtained in this study with those reported in the literature. A notable finding is that previous studies typically employ significantly higher doses of adsorbent materials, up to three times greater, compared to the 1.5 mg used in this study. This difference in dosage could explain the higher removal capacities reported in some studies [81,82].

4. Conclusion

The results indicate that both unactivated biochar (BC) and pre-trated biochar (BCA) are effective in the adsorption and degradation of the mycotoxin zearalenone (ZEN). Although BC exhibits a larger surface area and pore volume, BCA achieves more intense chemical interactions due to its increased surface functionalization resulting from the acid pretreatment. With an adsorption capacity of 64.96 μg g^{-1}, BCA slightly outperforms BC (60.23 μg g^{-1}) in ZEN removal, achieving efficiencies of 70 ± 5 % and 65 ± 5 %, respectively. The Freundlich model better describes the adsorption process in both materials, with BCA demonstrating a slight superiority in efficiency, particularly at lower temperatures. Regarding photodegradation, BCA also surpasses BC, achieving efficiencies greater than 97 % under UV irradiation, which is attributed to the additional hydroxyl groups present in BCA. Both materials exhibit high durability and regeneration capacity over 17–21 cycles, positioning them as promising options for advanced treatment of ZEN-contaminated water. The literature suggests that combining adsorption and photocatalysis processes can provide effective solutions for the removal of contaminants from aqueous media.

CRediT authorship contribution statement

J.C. Gómez-Vilchis: Writing – original draft, Investigation, Formal analysis. **G. García-Rosales:** Writing – review & editing, Writing – original draft, Supervision, Resources, Project administration, Methodology, Conceptualization. **L.C. Longoria-Gándara:** Validation, Conceptualization. **E.O. Pérez-Gómez:** Software. **D. Tenorio-Castilleros:** Software.

Data availability statement

"Data will be made available on request"

Ethical statement

"This study does not involve any human or animal subjects, and it is in accordance with research ethical standards"

Funding

"The authors declare that no funds, grants, or other support were received during the preparation of this manuscript".

Declaration of competing interest

The authors declare the following financial interests/personal relationships which may be considered as potential competing interests

G. Garcia-Rosales reports a relationship with National Technology of Mexico that includes: employment. If there are other authors, they declare that they have no known competing financial interests or personal relationships that could have appeared to influence the work reported in this paper.

Acknowledgements

The authors sincerely thank TECNM project 8257.20-P and the IAEA for their partial support of this research. J.C. Gómez-Vilchis also gratefully acknowledges the scholarship provided by CONAHCYT, Mexico.

References

[1] H. Wu, G. Xu, R. Yang, J. Dai, N.A. Al-Dhabi, G. Wang, L. Zhou, W. Tang, Responses of soil antibiotic resistance genes to the decrease in grain size of sediment discharged into Dongting Lake, China, Sci. Total Environ. 953 (2024) 176091, https://doi.org/10.1016/j.scitotenv.2024.176091.

[2] M.G. El -Desouky, A.A. Alayyafi, G.A.A.M. Al-Hazmi, A.A. El-Bindary, Effect of metal organic framework alginate aerogel composite sponge on adsorption of tartrazine from aqueous solutions: adsorption models, thermodynamics and optimization via Box-Behnken design, J. Mol. Liq. 399 (2024) 124392, https://doi.org/10.1016/j.molliq.2024.124392.

[3] H. Wu, G. Xu, R. Yang, J. Dai, N.A. Al-Dhabi, G. Wang, L. Zhou, W. Tang, Responses of soil antibiotic resistance genes to the decrease in grain size of sediment discharged into Dongting Lake, China, Sci. Total Environ. 953 (2024) 176091, https://doi.org/10.1016/j.scitotenv.2024.176091.

[4] M.G. El -Desouky, A.A. Alayyafi, G.A.A.M. Al-Hazmi, A.A. El-Bindary, Effect of metal organic framework alginate aerogel composite sponge on adsorption of tartrazine from aqueous solutions: adsorption models, thermodynamics and optimization via Box-Behnken design, J. Mol. Liq. 399 (2024) 124392, https://doi.org/10.1016/j.molliq.2024.124392.

[5] G.A.A. Al-Hazmi, M.A. El-Bindary, M.G. El-Desouky, A.A. El-Bindary, Efficient adsorptive removal of industrial dye from aqueous solution by synthesized zeolitic imidazolate framework-8 loaded date seed activated carbon and statistical physics modeling, Desalination Water Treat. 258 (2022) 85–103, https://doi.org/10.5004/dwt.2022.28397.

[6] A. Almahri, K.S. Abou-Melha, H.A. Katouah, A.M. Al-bonayan, F.A. Saad, M.G. El-Desouky, A.A. El-Bindary, Adsorption and removal of the harmful pesticide 2,4-dichlorophenylacetic acid from an aqueous environment via coffee waste biochar: synthesis, characterization, adsorption study and optimization via Box-Behnken design, J. Mol. Struct. 1293 (2023) 136238, https://doi.org/10.1016/j.molstruc.2023.136238.

[7] G.A.A. Al-Hazmi, A.A. El-Zahhar, M.G. El-Desouky, M.A. El-Bindary, A.A. El-Bindary, Efficiency of Fe_3O_4 @ZIF-8 for the removal of Doxorubicin from aqueous solutions: equilibrium, kinetics and thermodynamic studies, Environ. Technol. 45 (4) (2024) 731–750, https://doi.org/10.1080/09593330.2022.2121181.

[8] A. Almahri, M. Morad, M.M. Aljohani, N.M. Alatawi, F.A. Saad, H.M. Abumelha, M.G. El-Desouky, A.A. El-Bindary, Atrazine reclamation from an aqueous environment using a ruthenium-based metal-organic framework, Process Saf. Environ. Protect. 177 (2023) 52–68, https://doi.org/10.1016/j.psep.2023.06.091.

[9] G.A.A. Al-Hazmi, A.A. El-Zahhar, M.G. El-Desouky, M.A. El-Bindary, A.A. El-Bindary, Adsorption of industrial dye onto a zirconium metal-organic framework: synthesis, characterization, kinetics, thermodynamics, and DFT calculations, J. Coord. Chem. 75 (9–10) (2022) 1203–1229, https://doi.org/10.1080/00958972.2022.2114349.

[10] H.M. Nassef, G.A.A.M. Al-Hazmi, A.A. Alayyafi, M.G. El-Desouky, A.A. El-Bindary, Synthesis and characterization of new composite sponge combining of metal-organic framework and chitosan for the elimination of Pb (II), Cu(II) and Cd(II) ions from aqueous solutions: batch adsorption and optimization using Box-Behnken design, J. Mol. Liq. 394 (2024) 123741, https://doi.org/10.1016/j.molliq.2023.123741.

[11] A.M. Alsuhaibani, A.A. Alayyafi, L.A. Albedair, M.G. El-Desouky, A.A. El-Bindary, Efficient fabrication of a composite sponge for Cr (VI) removal via citric acid cross-linking of metal-organic framework and chitosan: adsorption isotherm, kinetic studies, and optimization using Box-Behnken design, Mater. Today Sustain. 26 (2024) 100732, https://doi.org/10.1016/j.mtsust.2024.100732.

[12] G.A.A. Al-Hazmi, M.A. El-Bindary, M.G. El-Desouky, A.A. El-Bindary, Efficient adsorptive removal of industrial dye from aqueous solution by synthesized zeolitic imidazolate framework-8 loaded date seed activated carbon and statistical physics modeling, Desalination Water Treat. 258 (2022) 85–103, https://doi.org/10.5004/dwt.2022.28397.

[13] Ahmadou Abderahim, Brun Nicolas, Napoli Alfredo, Durand Noel, Montet Didier, Effect of pyrolysis temperature on ochratoxin A adsorption mechanisms and kinetics by cashew nut shell biochars, SRDP J. Food Sci. Technol. 4 (7) (2019) 877–888, https://doi.org/10.25177/jfst.4.7.ra.565.

[14] A. Castell, N. Arroyo-Manzanares, N. Campillo, C. Torres, J. Fenoll, P. Viñas, Bioaccumulation of mycotoxins in human forensic liver and animal liver samples using a green sample treatment, Microchem. J. 185 (2023) 108192, https://doi.org/10.1016/j.microc.2022.108192.

[15] A. Zinedine, J.M. Soriano, J.C. Moltó, J. Mañes, Review on the toxicity, occurrence, metabolism, detoxification, regulations and intake of zearalenone: an oestrogenic mycotoxin, Food Chem. Toxicol. 45 (1) (2007) 1–18, https://doi.org/10.1016/j.fct.2006.07.030.

[16] A. Cimbalo, M. Alonso-Garrido, G. Font, L. Manyes, Toxicity of mycotoxins in vivo on vertebrate organisms: a review, Food Chem. Toxicol. 137 (2020) 111161, https://doi.org/10.1016/j.fct.2020.111161.

[17] G. Yang, Y. Wang, T. Wang, D. Wang, H. Weng, Q. Wang, C. Chen, Variations of enzymatic activity and gene expression in zebrafish (Danio rerio) embryos co-exposed to zearalenone and fumonisin B1, Ecotoxicol. Environ. Saf. 222 (2021) 112533, https://doi.org/10.1016/j.ecoenv.2021.112533.

[18] K. Gromadzka, A. Waśkiewicz, P. Goliński, J. Świetlik, Occurrence of estrogenic mycotoxin – zearalenone in aqueous environmental samples with various NOM content, Water Res. 43 (4) (2009), https://doi.org/10.1016/j.watres.2008.11.042.

[19] G. Wang, H. Wu, J. Dai, Y. Xiong, Y. Long, X. Cai, S. Mo, R. Yang, Y. Liu, Priorities identification of habitat restoration for migratory birds under the increased water level during the middle of dry season: a case study of Poyang Lake and Dongting Lake wetlands, China, Ecol. Indicat. 151 (2023) 110322, https://doi.org/10.1016/j.ecolind.2023.110322.

[20] Salhah H. Alrefaee, Meshari Aljohani, Kholood Alkhamis, Fathy Shaaban, Mohamed G. El-Desouky, Ashraf A. El-Bindary, Mohamed A. El-Bindary, Adsorption and effective removal of organophosphorus pesticides from aqueous solution via novel metal-organic framework: adsorption isotherms, kinetics, and optimization via Box-Behnken design, J. Mol. Liq. 384 (2023) 122206, https://doi.org/10.1016/j.molliq.2023.122206.

[21] X. Yang, J. Pan, J. Hu, S. Zhao, K. Cheng, MOF-derived La–$ZnFe_2O4$@Fe_3O_4@carbon magnetic hybrid composite as a highly efficient and recyclable photocatalyst for mycotoxins degradation, Chem. Eng. J. 467 (2023) 143381, https://doi.org/10.1016/j.cej.2023.143381.

[22] N. Zhang, X. Han, Y. Zhao, Y. Li, J. Meng, H. Zhang, J. Liang, Removal of aflatoxin B1 and zearalenone by clay mineral materials: in the animal industry and environment, Appl. Clay Sci. 228 (2022) 106614, https://doi.org/10.1016/j.clay.2022.106614.

[23] SIAP, Análisis Estadístico de la Producción [WWW Document], Serv. Inf. Agroaliment. y Pesq (2024). https://nube.siap.gob.mx/cierreagricola/. accessed 15.10.24.

[24] M.L. Dreher, A.J. Davenport, Hass avocado composition and potential health effects, Crit. Rev. Food Sci. Nutr. 53 (7) (2013), https://doi.org/10.1080/10408398.2011.556759.

[25] V. Mishra, M.K. Warshi, A. Sati, A. Kumar, V. Mishra, A. Sagdeo, R. Kumar, P.R. Sagdeo, Diffuse reflectance spectroscopy: an effective tool to probe the defect states in wide band gap semiconducting materials, Mater. Sci. Semicond. Process. 86 (2018) 151–156, https://doi.org/10.1016/j.mssp.2018.06.025.

[26] X. Lu, J. Zhao, Adsorption of ciprofloxacin on co-pyrolyzed biochar from fish scale and pine needle, Chin. J. Anal. Chem. 52 (1) (2024) 100350, https://doi.org/10.1016/j.cjac.2023.100350.

[27] V.J. Inglezakis, A.A. Zorpas, Heat of adsorption, adsorption energy and activation energy in adsorption and ion exchange systems, Desalination Water Treat. 39 (1–3) (2012) 149–157, https://doi.org/10.1080/19443994.2012.669169.

[28] C.-H. Tsai, W.-T. Tsai, L.-A. Kuo, Effect of Post-washing on textural characteristics of carbon materials derived from pineapple peel biomass, Materials 16 (24) (2023) 7529, https://doi.org/10.3390/ma16247529.

[29] S. Wongrod, A. Watcharawittaya, S. Vinitnantharat, Recycling of nutrient-loaded biochars produced from agricultural residues as soil promoters for Gomphrena growth. IOP Conference Series, Earth Environ. Sci. 463 (1) (2020) 012099, https://doi.org/10.1088/1755-1315/463/1/012099.

[30] Z. Zaitun, A. Halim, Y. Sa'dah, R. Cahyadi, Surface morphology properties of biochar feedstock for soil amendment. IOP Conference Series, Earth Environ. Sci. 951 (1) (2022) 012034, https://doi.org/10.1088/1755-1315/951/1/012034.

[31] J.C. Fernando, C. Peiris, C.M. Navarathna, S.R. Gunatilake, U. Welikala, S.T. Wanasinghe, S.B. Madduri, S. Jayasinghe, T.E. Mlsna, E.B. Hassan, F. Ferez, Nitric acid surface pre-modification of novel Lasia spinosa biochar for enhanced methylene blue remediation, Groundwater Sustain. Dev. 14 (2021) 100603, https://doi.org/10.1016/j.gsd.2021.100603.

[32] Y. Wang, B. Li, A. Gao, K. Ding, X. Xing, J. Wei, Y. Huang, J. Chun-Ho Lam, K.A. Subramanian, S. Zhang, Volatile-char interactions during biomass pyrolysis: effect of biomass acid-washing pretreatment, Fuel 340 (2023) 127496, https://doi.org/10.1016/j.fuel.2023.127496.

[33] S. Sutradhar, A. Mondal, F. Kuehne, O. Krueger, S.K. Rakshit, K. Kang, Comparison of oil-seed shell biomass-based biochar for the removal of anionic dyes-characterization and adsorption efficiency studies, Plants 13 (6) (2024) 820, https://doi.org/10.3390/plants13060820.

[34] K. Singh, H. Dave, B. Prasad, M. Kumari, D. Dubey, A.K. Rai, R. Ravi, J. Manjhi, M. Sillanpää, K.S. Prasad, nFeO decorated wood biochar as an adsorbent for aqueous Cr(VI) ions: hyphenated, coagulation-column treatment of tannery effluent, J. Water Proc. Eng. 59 (2024) 105084, https://doi.org/10.1016/j.jwpe.2024.105084.

[35] N. Van Vinh, M. Zafar, S.K. Behera, H.-S. Park, Arsenic(III) removal from aqueous solution by raw and zinc-loaded pine cone biochar: equilibrium, kinetics, and thermodynamics studies, Int. J. Environ. Sci. Technol. 12 (4) (2015) 1283–1294, https://doi.org/10.1007/s13762-014-0507-1.

[36] M.R. Yazdani, N. Duimovich, A. Tiraferri, P. Laurell, M. Borghei, J.B. Zimmerman, R. Vahala, Tailored mesoporous biochar sorbents from pinecone biomass for the adsorption of natural organic matter from lake water, J. Mol. Liq. 291 (2019) 111248, https://doi.org/10.1016/j.molliq.2019.111248.

[37] B.M. Córdova, J.P. Santa Cruz, M.T.v. Ocampo, R.G. Huamani-Palomino, A.M. Baena-Moncada, Simultaneous adsorption of a ternary mixture of brilliant green, rhodamine B and methyl orange as artificial wastewater onto biochar from cocoa pod husk waste. Quantification of dyes using the derivative spectrophotometry method, New J. Chem. 44 (20) (2020) 8303–8316, https://doi.org/10.1039/d0nj00916d.

[38] G. Huang, M. Wang, Q. Liu, S. Zhao, H. Liu, F. Liu, J. Liu, Efficient removal of tetracycline in water using modified eggplant straw biochar supported green nanoscale zerovalent iron: synthesis, removal performance, and mechanism, RSC Adv. 14 (5) (2024) 3567–3577, https://doi.org/10.1039/D3RA08417E.

[39] B. D'Cruz, M. Madkour, M.O. Amin, E. Al-Hetlani, Efficient and recoverable magnetic AC-Fe3O4 nanocomposite for rapid removal of promazine from wastewater, Mater. Chem. Phys. 240 (2020) 122109, https://doi.org/10.1016/j.matchemphys.2019.122109.

[40] N. Welter, J. Leichtweis, S. Silvestri, P.I.Z. Sánchez, A.C.C. Mejía, E. Carissimi, Preparation of a new green composite based on chitin biochar and $ZnFe_2O_4$ for photo-Fenton degradation of Rhodamine B, J. Alloys Compd. 901 (2022) 163758, https://doi.org/10.1016/j.jallcom.2022.163758.

[41] L. Meng, W. Yin, S. Wang, X. Wu, J. Hou, W. Yin, K. Feng, Y.S. Ok, X. Wang, Photocatalytic behavior of biochar-modified carbon nitride with enriched visible-light reactivity, Chemosphere 239 (2020) 124713, https://doi.org/10.1016/j.chemosphere.2019.124713.

[42] A. Bakry, M.S.A. Darwish, T.F. Hassanein, Adsorption of methylene blue from aqueous solutions using carboxyl/nitro-functionalized microparticles derived from polypropylene waste, Iran. Polym. J. (Engl. Ed.) 31 (2) (2022) 185–197, https://doi.org/10.1007/s13726-021-00979-w.

[43] Z. Ying, D. Zhao, H. Li, X. Liu, J. Zhang, Efficient adsorption of deoxynivalenol by porous carbon prepared from soybean dreg, Toxins 13 (7) (2021) 500, https://doi.org/10.3390/toxins13070500.

[44] L. Azeez, O. Adefunke, A.O. Oyedeji, B.K. Agbaogun, H.K. Busari, A.L. Adejumo, W.B. Agbaje, A.E. Adeleke, A.O. Samuel, Facile removal of rhodamine B and metronidazole with mesoporous biochar prepared from palm tree biomass: adsorption studies, reusability, and mechanisms, Water Pract. Technol. 19 (3) (2024) 730–744, https://doi.org/10.2166/wpt.2024.049.

[45] M.L. Brusseau, J. Chorover, Chemical processes affecting contaminant transport and fate, Environ. Pollut. Sci. (2019) 113–130, https://doi.org/10.1016/b978-0-12-814719-1.00008-2.

[46] A. Fatemeh, M. Gholami, A. Jonidi, M. Kermani, H. Asgharnia, R. Rezaeikalantari, Study of tetracycline and metronidazole adsorption on biochar prepared from rice bran kinetics, isotherms and mechanisms, Desalination Water Treat. 159 (2019) 390–401, https://doi.org/10.5004/dwt.2019.24140.

[47] M. Marković, A. Daković, G.E. Rottinghaus, A. Petković, M. Kragović, D. Krajišnik, J. Milić, Ochratoxin A and zearalenone adsorption by the natural zeolite treated with benzalkonium chloride, Colloids Surf. A Physicochem. Eng. Asp. 529 (2017), https://doi.org/10.1016/j.colsurfa.2017.05.054.

[48] V. Gajendiran, P. Deivasigamani, S. Sivamani, S. Banerjee, Biochar from Manihot esculenta stalk as potential adsorbent for removal of reactive yellow dye, Desalination Water Treat. (2024) 100120, https://doi.org/10.1016/j.dwt.2024.100120.

[49] P. Pourhakkak, A. Taghizadeh, M. Taghizadeh, M. Ghaedi, S. Haghdoust, Chapter 1-Fundamentals of adsorption technology, Interface Sci. Technol. 33 (2021) 1–70, https://doi.org/10.1016/B978-0-12-818805-7.00001-1. Elsevier.

[50] Y. Hu, C. Ma, W. Huang, S. Guo, T. Wang, J. Liu, Adsorption behavior of activated carbon for the elimination of zearalenone during bleaching process of corn oil, Grain & Oil Science and Technology 6 (1) (2023) 24–33, https://doi.org/10.1016/j.gaost.2022.11.002.

[51] H. Freundlich, Über die Adsorption in Lösungen, Z. Phys. Chem. 57U (1) (1907) 385–470, https://doi.org/10.1515/zpch-1907-5723.

[52] G. Chu, J. Zhao, Y. Huang, D. Zhou, Y. Liu, M. Wu, H. Peng, Q. Zhao, B. Pan, C.E.W. Steinberg, Phosphoric acid pretreatment enhances the specific surface areas of biochars by generation of micropores, Environ. Pollut. 240 (2018) 1–9, https://doi.org/10.1016/j.envpol.2018.04.003.

[53] L. Li, S. Xiaoxue, Z. Yuchong, W. Jin, L. Zilong, G. Yuxi, C. Shuai, J. Youjun, C. Jinying, Application in photocatalytic degradation of zearalenone based on graphitic carbon nitride, Luminescence 37 (2) (2022) 190–198, https://doi.org/10.1002/bio.4160.

[54] N. Daneshvar, M. Rabbani, N. Modirshahla, M.A. Behnajady, Kinetic modeling of photocatalytic degradation of Acid Red 27 in UV/TiO_2 process, J. Photochem. Photobiol. Chem. 168 (1–2) (2004) 39–45, https://doi.org/10.1016/j.jphotochem.2004.05.011.

[55] N. Barka, A. Assabbane, A. Nounah, Y.A. Ichou, Photocatalytic degradation of indigo carmine in aqueous solution by TiO_2-coated non-woven fibres, J. Hazard Mater. 152 (3) (2008) 1054–1059, https://doi.org/10.1016/j.jhazmat.2007.07.080.

[56] H. Zhang, G. Chen, D.W. Bahnemann, Photoelectrocatalytic materials for environmental applications, J. Mater. Chem. 19 (29) (2009) 5089, https://doi.org/10.1039/b821991e.

[57] J. Fan, Y. Guo, J. Wang, M. Fan, Rapid decolorization of azo dye methyl orange in aqueous solution by nanoscale zerovalent iron particles, J. Hazard Mater. 166 (2) (2009) 904–910, https://doi.org/10.1016/j.jhazmat.2008.11.091.

[58] H.-Y. Shu, M.-C. Chang, H.-H. Yu, W.-H. Chen, Reduction of an azo dye Acid Black 24 solution using synthesized nanoscale zerovalent iron particles, J. Colloid Interface Sci. 314 (1) (2007) 89–97, https://doi.org/10.1016/j.jcis.2007.04.071.

[59] Y.-W. Chen, Y.-H. Hsu, Effects of reaction temperature on the photocatalytic activity of TiO_2 with Pd and Cu cocatalysts, Catalysts 11 (8) (2021) 966, https://doi.org/10.3390/catal11080966.

[60] N. Acelas, S.M. Lopera, J. Porras, R.A. Torres-Palma, Evaluating the removal of the antibiotic cephalexin from aqueous solutions using an adsorbent obtained from palm oil fiber, Molecules 26 (11) (2021) 3340, https://doi.org/10.3390/molecules26113340.

[61] E.E.P. Ramírez, M.L. Asunción, V.S. Rivalcoba, A.L.M. Hernández, C.V. Santos, Removal of phenolic compounds from water by adsorption and photocatalysis, in: Phenolic Compounds-Natural Sources, Importance and Applications, InTech, 2017, https://doi.org/10.5772/66895.

[62] G. Wang, Y. Miao, Z. Sun, S. Zheng, Simultaneous adsorption of aflatoxin B1 and zearalenone by mono- and di-alkyl cationic surfactants modified montmorillonites, J. Colloid Interface Sci. 511 (2018) 67–76, https://doi.org/10.1016/j.jcis.2017.09.074.

[63] A. Daković, S. Matijašević, G.E. Rottinghaus, V. Dondur, T. Pietrass, C.F.M. Clewett, Adsorption of zearalenone by organomodified natural zeolitic tuff, J. Colloid Interface Sci. 311 (1) (2007) 8–13, https://doi.org/10.1016/j.jcis.2007.02.033.

[64] Y. Seki, K. Yurdakoç, Adsorption of promethazine hydrochloride with KSF montmorillonite, Adsorption 12 (1) (2006) 89–100, https://doi.org/10.1007/s10450-006-0141-4.

[65] B. Ohtani, Revisiting the fundamental physical chemistry in heterogeneous photocatalysis: its thermodynamics and kinetics, Phys. Chem. Chem. Phys. 16 (5) (2014) 1788–1797, https://doi.org/10.1039/c3cp53653j.

[66] Y. Fan, L. Huang, L. Wu, C. Zhang, S. Zhu, X. Xiao, M. Li, X. Zou, Adsorption of sulfonamides on biochars derived from waste residues and its mechanism, J. Hazard Mater. 406 (2021) 124291, https://doi.org/10.1016/j.jhazmat.2020.124291.

[67] S. Yu, L. Wu, J. Ni, H. Zhang, R. Wei, W. Chen, The chemical compositions and carbon structures of pine sawdust- and wheat straw-derived biochars produced in air-limitation, carbon dioxide, and nitrogen atmospheres, and their variation with charring temperature, Fuel 122852 (2021), https://doi.org/10.1016/j.fuel.2021.122852.

[68] H.-O. Chahinez, O. Abdelkader, Y. Leila, H.N. Tran, One-stage preparation of palm petiole-derived biochar: characterization and application for adsorption of crystal violet dye in water, Environ. Technol. Innovat. 19 (2020) 100872, https://doi.org/10.1016/j.eti.2020.100872.

[69] C. Peiris, S. Nawalage, J.J. Wewalwela, S.R. Gunatilake, M. Vithanage, Biochar based sorptive remediation of steroidal estrogen contaminated aqueous systems: a critical review, Environ. Res. 191 (2020) 110183, https://doi.org/10.1016/j.envres.2020.110183.

[70] S. Maldonado, S. Morin, K.J. Stevenson, Structure, composition, and chemical reactivity of carbon nanotubes by selective nitrogen doping, Carbon 44 (8) (2006) 1429–1437, https://doi.org/10.1016/j.carbon.2005.11.027.

[71] D. Guo, R. Shibuya, C. Akiba, S. Saji, T. Kondo, J. Nakamura, Active sites of nitrogen-doped carbon materials for oxygen reduction reaction clarified using model catalysts, Science 351 (6271) (2016) 361–365, https://doi.org/10.1126/science.aad0832.

[72] Q. Wu, Y. Zhang, M. Cui, H. Liu, H. Liu, Z. Zheng, W. Zheng, C. Zhang, D. Wen, Pyrolyzing pharmaceutical sludge to biochar as an efficient adsorbent for deep removal of fluoroquinolone antibiotics from pharmaceutical wastewater: performance and mechanism, J. Hazard Mater. 426 (2022) 127798, https://doi.org/10.1016/j.jhazmat.2021.127798.
[73] H. Xiong, J. Chen, T. Zhang, W. Wang, C. Huang, Y. Zhu, B. Hu, Unexpected ultrafast elimination of uranium and europium from aqueous solutions with magnetic bio-$CaCO_3$, J. Mol. Liq. 322 (2021) 114986, https://doi.org/10.1016/j.molliq.2020.114986.
[74] Z. Sun, C. Lian, C. Li, S. Zheng, Investigations on organo-montmorillonites modified by binary nonionic/zwitterionic surfactant mixtures for simultaneous adsorption of aflatoxin B1 and zearalenone, J. Colloid Interface Sci. 565 (2020) 11–22, https://doi.org/10.1016/j.jcis.2020.01.013.
[75] J.W. Peterson, L.J. Petrasky, M.D. Seymour, R.S. Burkhart, A.B. Schuiling, Adsorption and breakdown of penicillin antibiotic in the presence of titanium oxide nanoparticles in water, Chemosphere 87 (8) (2012) 911–917, https://doi.org/10.1016/j.chemosphere.2012.01.044.
[76] J.E. Cevallos-Mendoza, J.S. Cedeño-Muñoz, J.M. Navia-Mendoza, F. Figueira, C.G. Amorim, J.M. Rodríguez-Díaz, M.C.B.S.M. Montenegro, Development of hybrid MIL-53(Al)@CBS for ternary adsorption of tetracyclines antibiotics in water: physical interpretation of the adsorption mechanism, Bioresour. Technol. 396 (2024) 130453, https://doi.org/10.1016/j.biortech.2024.130453.
[77] M. Spasojević, A. Daković, G.E. Rottinghaus, M. Obradović, D. Krajišnik, M. Marković, J. Krstić, Influence of surface coverage of kaolin with surfactant ions on adsorption of ochratoxin A and zearalenone, Appl. Clay Sci. 205 (2021) 106040, https://doi.org/10.1016/j.clay.2021.106040.
[78] H. Liang, C. Zhu, A. Wang, F. Chen, Facile preparation of NiFe2O4/biochar composite adsorbent for efficient adsorption removal of antibiotics in water, Carbon Research 3 (1) (2024) 2, https://doi.org/10.1007/s44246-023-00094-w.
[79] K.A. Azalok, A.A. Oladipo, M. Gazi, UV-light-induced photocatalytic performance of reusable MnFe-LDO–biochar for tetracycline removal in water, J. Photochem. Photobiol. Chem. 405 (2021) 112976, https://doi.org/10.1016/j.jphotochem.2020.112976.
[80] H. Peng, L. Wang, X. Zheng, Efficient adsorption-photodegradation activity of MoS2 coupling with S, N-codoped porous biochar derived from chitosan, J. Water Proc. Eng. 51 (2023) 103426, https://doi.org/10.1016/j.jwpe.2022.103426.
[81] N. Jagadeesh, B. Sundaram, Adsorption of pollutants from wastewater by biochar: a review, J. Hazard. Mater. Advan. 9 (2023) 100226, https://doi.org/10.1016/j.hazadv.2022.100226.
[82] G. Murtaza, Z. Ahmed, D.-Q. Dai, R. Iqbal, S. Bawazeer, M. Usman, M. Rizwan, J. Iqbal, M.I. Akram, A.S. Althubiani, A. Tariq, I. Ali, A review of mechanism and adsorption capacities of biochar-based engineered composites for removing aquatic pollutants from contaminated water, Front. Environ. Sci. 10 (2022), https://doi.org/10.3389/fenvs.2022.1035865.
[83] W. Zhang, L. Zhang, X. Jiang, X. Liu, Y. Li, Y. Zhang, Enhanced adsorption removal of aflatoxin B1, zearalenone and deoxynivalenol from dairy cow rumen fluid by modified nano-montmorillonite and evaluation of its mechanism, Anim. Feed Sci. Technol. 259 (2020) 114366, https://doi.org/10.1016/j.anifeedsci.2019.114366.
[84] Z.M. Bekci, M.K. Antep, M. Merdivan, K. Yurdakoç, Zearalenone removal in synthetic media and aqueous part of canned corn by montmorillonite K10 and pillared montmorillonite K10, J. Food Protect. 74 (6) (2011) 954–959, https://doi.org/10.4315/0362-028X.JFP-10-317.
[85] X. Bai, C. Sun, D. Liu, X. Luo, D. Li, J. Wang, N. Wang, X. Chang, R. Zong, Y. Zhu, Photocatalytic degradation of deoxynivalenol using graphene/ZnO hybrids in aqueous suspension, Appl. Catal. B Environ. 204 (2017) 11–20, https://doi.org/10.1016/j.apcatb.2016.11.010.
[86] M.S. Samuel, K. Mohanraj, N. Chandrasekar, R. Balaji, E. Selvarajan, Synthesis of recyclable GO/Cu3(BTC)2/Fe3O4 hybrid nanocomposites with enhanced photocatalytic degradation of aflatoxin B1, Chemosphere 291 (2022) 132684, https://doi.org/10.1016/j.chemosphere.2021.132684.
[87] X. Chen, B. Chu, Q. Gu, H. Liu, C. Li, W. Li, J. Lu, D. Wu, Facile fabrication of protonated g-C3N4/oxygen-doped g-C3N4 homojunction with enhanced visible photocatalytic degradation performance of deoxynivalenol, J. Environ. Chem. Eng. 9 (6) (2021) 106380, https://doi.org/10.1016/j.jece.2021.106380.